APPLICATIONS OF
MODELLING AND SIMULATION
http://arqiipubl.com/ams eISSN 2600-8084 VOL 9, 2025, 92-106

Design and Optimization of Π-Shaped Slotted Dual-Band SIW Antenna for 5G Applications

Md Mahabub Alam[1], Nurhafizah Abu Talip Yusof[1,2*], Yasmin Abdul Wahab[1], Mohamad Shaiful Abdul Karim[1] and Md. Suaibur Rahman[3]

[1]Faculty of Electrical and Electronics Engineering Technology, Universiti Malaysia Pahang Al-Sultan Abdullah, 26600 Pekan, Pahang, Malaysia
[2]Centre of Research in Advanced Fluid and Processes (Fluid Center), Universiti Malaysia Pahang Al-Sultan Abdullah, Leburaya Tun Khalil Yaakob, 26300 Kuantan, Pahang, Malaysia
[3]Department of Electrical and Electronics Engineering Technology, Islamic University of Technology, Gazipur-1704, Dhaka, Bangladesh

*Corresponding author: hafizahs@umpsa.edu.my

Submitted 13 October 2024, Revised 30 January 2025, Accepted 03 February 2025, Available online 14 March 2025.

Abstract: This paper presents the design and optimization of a dual-band, linearly polarized Substrate-Integrated Waveguide (SIW) antenna for 5G base stations, addressing challenges such as increased path loss and interference at millimeter-wave (mm-wave) frequencies. The innovation lies in a Π-shaped slotted SIW structure, enabling wideband operation across the 28 GHz and 38 GHz bands. Two longitudinal slots and one transversal slot, etched on a Rogers 5880 substrate, are strategically optimized to achieve dual-band performance. The antenna achieves a bandwidth of 1.786 GHz (27.491 - 29.277 GHz) for the 28 GHz band and 683 MHz (37.496 - 38.179 GHz) for the 38 GHz band. Simulations conducted using Computer Simulation Technology (CST) Microwave Studio software indicate gains of 7.9 dB and 8.05 dB, beamwidths of 64.1° and 61.7°, and radiation efficiencies of 94.83% and 92.61% at 28 GHz and 38 GHz, respectively. To validate the design, an Artificial Neural Network (ANN) model was employed, achieving high predictive accuracy with R^2 values of 0.98 for resonance frequency and 0.972 for gain. Compared to prior works, the proposed antenna offers enhanced gain, efficiency, and bandwidth, making it a promising solution for mm-wave 5G applications.

Keywords: Antenna design; Dual-band; Optimization; SIW antenna; 5G; Π-shaped.

1. INTRODUCTION

The transition to millimetre-wave (mm-wave) frequencies is critical for advancing wireless communication networks, particularly in addressing the high data rate and traffic capacity demands of 5G mobile communications. These frequencies, ranging from 24 GHz to 300 GHz, are pivotal in supporting innovative applications. Among them, the 28 GHz (27.5 - 29.5 GHz) and 38 GHz (37 - 40 GHz) bands stand out due to their optimal balance between telecommunications and high-speed data transmission characteristics. These bands play a crucial role in enhancing 5G system performance by overcoming key challenges of 4G networks, such as high latency and limited coverage [1-4].

Multiband antennas have emerged as efficient solutions for 5G communications, enabling coverage of multiple frequency ranges within a single device. However, the mm-wave spectrum poses inherent challenges, such as significant path loss and limited scattering caused by environmental factors like rain, fog, and humidity [5-7]. To mitigate these effects and ensure reliable performance, high-gain antennas with wide bandwidths and high efficiency are indispensable. Despite various advancements, many existing dual-band antenna designs struggle with performance trade-offs, often prioritizing one frequency band at the expense of the other. This results in reduced bandwidth or compromised gain in one of the bands, necessitating innovative solutions that can achieve balanced performance across both [12-15].

Substrate-Integrated Waveguide (SIW) technology has emerged as a compelling approach to overcoming these challenges. By embedding metallic vias or plated through-holes within a dielectric substrate, SIW structures replicate the properties of conventional waveguides while offering the compactness and ease of integration associated with planar antennas. SIW antennas are characterized by low loss, high efficiency, excellent isolation, and reduced surface wave losses, making them ideal for 5G mm-wave applications [8–11]. Several dual-band SIW antennas for 5G mm-wave applications have been introduced [16-18], yet many exhibit trade-offs between gain, bandwidth, and efficiency. For instance, the slotted SIW antennas in [12-13] demonstrated enhanced radiation efficiency but were limited by bandwidths of less than 1 GHz. Similarly, the designs in [14–15] achieved dual-band operation but encountered challenges related to lower gain, with maximum values

falling below 7 dBi, particularly in high-frequency environments. These shortcomings highlight the need for further research to develop designs that simultaneously maximize gain, bandwidth, and efficiency.

This work addresses these gaps by introducing a Π-shaped slotted dual-band SIW antenna optimized for operation at 28 GHz and 38 GHz. The proposed design incorporates two longitudinal slots and one transversal slot, forming new resonant topologies that significantly enhance antenna performance across both frequency bands. Using simulation-based parameter optimization, the design achieves wide bandwidths exceeding 2 GHz and high broadside gains surpassing 8 dBi while maintaining excellent radiation efficiency. Unlike previous designs, which often require additional steps to balance gain and bandwidth [12-15], the proposed antenna demonstrates a superior balance across these metrics, offering a more effective solution for 5G mm-wave communications.

The paper is structured as follows: Section 2 explores the working principle of the dual-band SIW microstrip antenna. Section 3 details the antenna design methodology, while Section 4 presents the performance metrics results and the validation of the proposed antenna design using an Artificial Neural Network (ANN) approach. Section 5 highlights the antenna's advantages through a comparative analysis with previous works, demonstrating its superior performance. Finally, Section 6 concludes with insights into the antenna's potential for real-world 5G mm-wave applications.

2. WORKING PRINCIPLE

The design of SIW microstrip patch antennas represents a significant advancement in antenna technology, combining the advantages of conventional microstrip antennas with those of waveguide structures. This hybrid design integrates waveguide-like functionality directly into a planar substrate, resulting in a compact, low-profile antenna with enhanced performance characteristics. As shown in Figure 1(a), a microstrip patch antenna consists of a thin metallic radiator, typically rectangular or circular, situated on a dielectric substrate, with a conductive ground plane located beneath. Excitation methods, such as coaxial probes or microstrip lines, enable low-profile, cost-effective designs suitable for various wireless communication applications. The resonant frequency of the antenna is determined by the dimensions of the patch and the properties of the substrate. The structure forms a resonant cavity that primarily radiates through fringing fields at the edges of the patch. Figure 1(b) illustrates how the SIW integrates waveguide functionality into the substrate through parallel rows of metallic vias. In this configuration, the ground plane and patch antenna serve as the bottom and top conductive boundaries, respectively [20]. SIW structures, composed of a dielectric substrate enclosed by two conductive plates, emulate the behavior of dielectric-filled waveguides by strategically placing metallic via arrays. This design approach allows SIWs to maintain a planar profile, in contrast to conventional rectangular waveguides, which are inherently three-dimensional. In SIW structures, only the transverse electric (TE) modes are permitted to propagate, as the metal vias along the sides obstruct the current flow necessary for the transverse magnetic (TM) modes [21].

The SIW antenna design relies on classical rectangular waveguide analysis, with the cut-off frequency for rectangular waveguide modes defined by Equation (1). f_c represents the cutoff frequency for various modes in a rectangular waveguide, c is the speed of light in a vacuum, m, and n are the mode numbers, and a and b are the equivalent length and width of the waveguide, respectively.

$$f_c = \frac{c}{2\pi}\sqrt{(\frac{m\pi}{a})^2 + (\frac{n\pi}{b})^2} \tag{1}$$

For the SIW antenna, the cutoff frequency for the TE mode (m = 1, n = 0) is given by Equation (2).

$$f_c = \frac{c}{2a} \tag{2}$$

The width of the dielectric-filled waveguide is critical, as it signifies the effective width of a waveguide filled with dielectric material instead of air. This parameter is crucial for predicting and optimizing SIW performance, as it directly influences wave propagation characteristics, including cutoff frequency and impedance, which are modified by the dielectric substrate. The dielectric-filled waveguide width, denoted as a_d, is defined by Equation (3) [20].

$$a_d = \frac{a}{\sqrt{\varepsilon_r}} \tag{3}$$

where ε_r is the relative permittivity (dielectric constant) of the filling material.

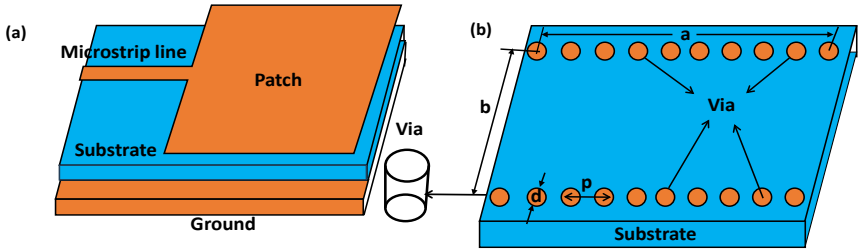

Figure 1. (a) Microstrip patch antenna and (b) basic geometry of SIW structure.

The effective width of SIW is a significant parameter that accounts for the electromagnetic field distribution within the structure. Due to fringing fields, it is slightly narrower than the distance between via rows. This parameter is necessary for accurately determining the cut-off frequencies and other waveguide characteristics within the SIW, as expressed in Equation (4) [19].

$$a_s = a_d + \frac{d}{0.98p} \tag{4}$$

In Equation (4), d is the via diameter and p is the space between the vias. To minimize losses in an SIW, the selection of via diameter and inter-via spacing must adhere to specific design criteria determined by Equation (5) that optimize electromagnetic wave confinement and reduce radiation leakage [22].

$$d < \lambda_g/5 \text{ and } p \leq 2d \tag{5}$$

where λ_g is the wavelength within the waveguide.

3. DESIGN METHODOLOGY

3.1 Π-Shaped Slotted SIW Antenna Design

The proposed design introduces a Π-shaped slotted SIW antenna optimized for 28 GHz and 38 GHz frequencies. The antenna is built on an RT/Duroid 5880 substrate (relative permittivity, ε_r= 2.2, and thin profile, h = 0.254 mm) with supported by an 18.4 mm patch radiator. The significant parameter modifications involve adding two longitudinal slots (7.8 mm × 0.70 mm) and one transversal slot (3.10 mm × 0.68 mm) to the patch, which optimizes current distribution and significantly broadens the operational bandwidth, making it ideal for 5G applications. The detailed configuration of the Π-shaped slotted SIW antenna is presented in Table 1.

For validation, the L-shaped slotted patch antenna design from Singh et al. [24] was first replicated and simulated using Computer Simulation Technology (CST) Microwave Studio software. Two configurations were tested: (a) the L-shaped slotted patch antenna without SIW and (b) the L-shaped slotted patch antenna with SIW integration, as shown in Figure 2(a) and 2(b), respectively. A 3D exploded view of the L-shaped slotted patch antenna with SIW is provided in Figure 2(c). These configurations were used as benchmarks for comparison and to verify the proposed methodology. The performance of the Π-shaped slotted SIW antenna, shown in Figure 2(d), will be compared with the reference L-shaped designs in Section 4, where the improvements in bandwidth, radiation efficiency, and gain will be presented in detail. The modifications to the antenna geometry demonstrate substantial enhancements, underscoring its suitability for 5G applications.

3.2 Parametric Optimization

3.2.1 Effects of Varying Dimensions on Longitudinal and Transversal Slots on Antenna Performance

Figure 3(a) illustrates the parametric analysis conducted to investigate the impact of varying the dimensions of longitudinal and transversal slots on antenna performance. The objective was to determine the optimal slot configuration for achieving superior antenna characteristics such as enhanced bandwidth, gain, and efficiency. Singh et al. [24] emphasized the critical role of slot geometry in determining the electromagnetic behavior of SIW antennas, highlighting the need for optimization. The analysis systematically examined the first longitudinal slot, the second longitudinal slot, and the transversal slot. The length of the first longitudinal slot (L_1) was varied from 7.78 mm to 7.86 mm, while its width (W_1) was adjusted between 0.66 mm and 0.72 mm. For the second longitudinal slot (L_2), the length ranged from 7.70 mm to 8.00 mm, and the width (W_2) varied from 0.60 mm to 0.90 mm. The transversal slot (L_3) had its length modified between 3.0 mm and 3.2 mm, with the width (W_3) adjusted from 0.68 mm to 0.78 mm. The parametric analysis was conducted using simulations to assess how these dimensional variations affected antenna performance. The study found that variations in the longitudinal slot dimensions influenced resonant frequency and bandwidth, while adjustments to the transversal slot dimensions impacted impedance matching and radiation efficiency. Based on these findings, the optimal slot dimensions were identified and used for further design refinement in the subsequent steps of the antenna optimization.

Table 1. Design parameters for the Π-shaped SIW antenna.

Define variables	Variable's description	Optimized value (mm)
W_g	Antenna width	7.50
L_g	Antenna length	27.00
d	Via diameter of SIW	0.50
W_f , L_f	Width and length of microstrip feed	0.37, 3.50
L_1 , W_1	Length and width of Slot 1	7.80, 0.70
L_2 , W_2	Length and width of Slot 2	7.80, 0.70
L_3 , W_3	Length and width of Slot 3	3.10, 0.68

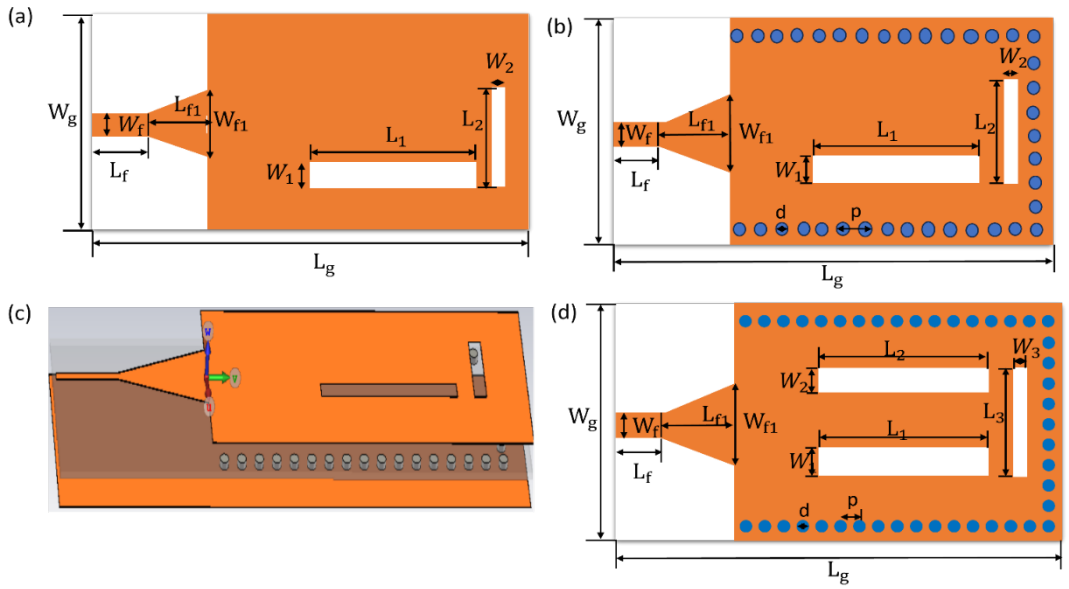

Figure 2. Validation technique analysis: (a) Slotted patch antenna without SIW, (b) Slotted patch antenna with SIW, (c) 3D exploded view of the slotted patch antenna with SIW [24], and (d) Π-shaped slotted SIW antenna design.

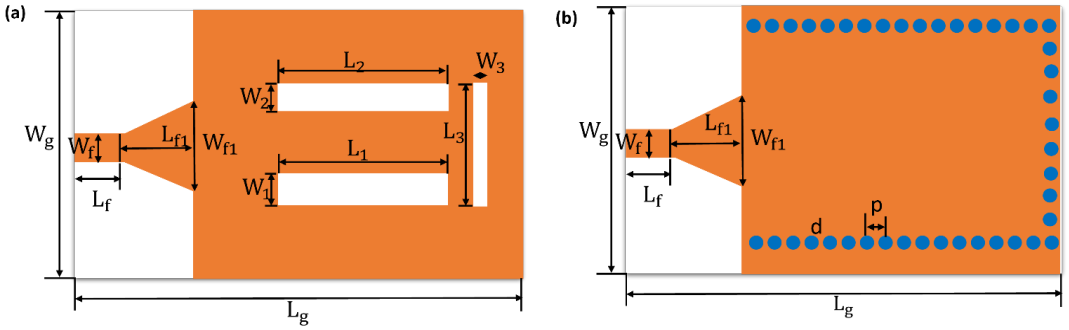

Figure 3. Parametric analysis of varying (a) lengths and widths of slots L_1, L_2, L_3 and W_1, W_2, W_3 and (b) diameter of vias (d).

3.2.2 Optimization of Via Diameter Variation on Antenna Performance

The subsequent stage of the parametric study focused on how varying the via diameter influences the performance of the Π-shaped slotted SIW antenna. The analysis was conducted by systematically changing the via diameter while keeping all other design elements fixed to isolate its specific impact. Figure 3(b) depicts the investigation, which explored three different via diameters measuring 0.4 mm, 0.5 mm, and 0.6 mm. This study aimed to understand how the size of the vias affects significant parameters such as impedance matching, signal propagation, and the structural stability of the antenna. According to Zhang et al. [23], via diameter plays a crucial role in maintaining electromagnetic properties and ensuring mechanical robustness in SIW antennas. The findings from this parametric investigation were essential for identifying the most suitable via diameter, which was later implemented in the final design of the Π-shaped slotted SIW antenna to achieve optimal performance for 5G communication systems.

3.3 Optimized Π-Shaped Slotted SIW Antenna Configuration

Figure 4 illustrates the optimized design of the dual-band SIW-based microstrip antenna. As noted in [25], the design was refined through a methodical optimization process by adjusting various SIW antenna parameters to achieve an effective SIW-based microstrip antenna suitable for 5G applications. The RT/Duroid 5880 single-layer substrate, which has a substrate thickness of 0.254 mm and a relative permittivity (ε_r) of 2.2, and a loss tangent (tan δ) of 0.0009 is used in the design of the proposed dual-band SIW antenna (Figure 4). The metalized via holes, 0.50 mm in diameter and spaced 1 mm center-to-center, form the SIW structure. A ratio of via pitch to via diameter (P/d) ratio below 2.5 is maintained to ensure optimal SIW performance. Three slots are etched into the metallic plane of the SIW structure to enhance antenna performance. Slots 1 and 2 are longitudinal, with dimensions L_1, W_1 and L_2,W_2, respectively, while Slot 3 is transverse, with L_3 and W_3. A 50-Ω microstrip line, positioned on the opposite side of the substrate, feeds the antenna via proximity coupling. The feed has a length (L_f) of 3.50 mm and a width (W_f) of 0.37 mm to ensure proper impedance matching. Three slots with lengths of 7.9 mm, 7.72 mm, and 3.1 mm and a uniform width of 0.7 mm are used to fine-tune the antenna's frequency response. A microstrip-to-SIW transition section is incorporated to achieve optimal impedance matching, with dimensions W_{f1} (width) and L_{f1} (length) between the feed line and the SIW structure. The complete antenna measures 27 mm by 7.5 mm, as specified in Table 2.

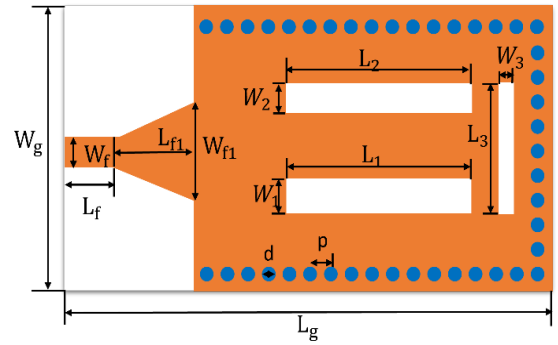

Figure 4. Optimized design of Π-shaped slotted SIW antenna.

Table 2. Optimized Π-Shaped Slotted SIW antenna design's dimensions.

Define variables	Variable's description	Optimized value [mm]
W_g	Antenna width	7.50
L_g	Antenna length	27.00
d	Via diameter of SIW	0.50
W_f , L_f	Width and length of microstrip feed	0.37, 3.50
L_1 , W_1	Length and width of Slot 1	7.90, 0.70
L_2 , W_2	Length and width of Slot 2	7.72, 0.70
L_3 , W_3	Length and width of Slot 3	3.10, 0.70

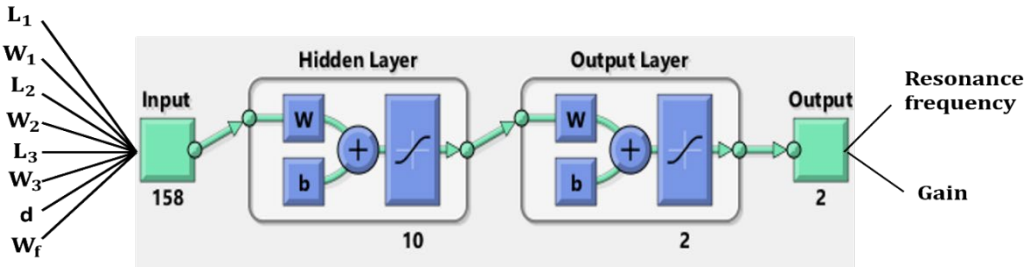

Figure 5. ANN architecture layers model.

3.4 Performance Validation Using ANN Model

To validate the performance of the proposed antenna design, an Artificial Neural Network (ANN) model was employed. The ANN model is designed to predict significant antenna parameters and consists of an input layer with 8 neurons, a hidden layer with 10 neurons, and an output layer with two neurons, as shown in Figure 5. The input layer processes eight crucial antenna parameters, including the dimensions of the longitudinal and transversal slots, via diameter, feeding width, and four additional input parameters. The hidden layer, containing 10 neurons, serves as the computational core, where complex relationships between inputs are processed using appropriate activation functions and weight adjustments during training. The output layer produces two essential antenna performance metrics, optimized for the 28 GHz and 38 GHz frequency bands.

The ANN model was trained using a dataset generated from CST Microwave Studio simulations, ensuring accurate predictions of the antenna's performance metrics. The parameters obtained from this approach include resonance frequency and gain for both the 28 GHz and 38 GHz frequency bands. The validation results include R-squared (R^2) values, Mean Square Error (MSE), and Root Mean Square Error (RMSE), which demonstrate the model's predictive accuracy. These validation results will be presented in the results section to confirm the effectiveness of the ANN model in predicting the antenna's performance. This method provides a robust framework for performance validation, ensuring that the proposed antenna design meets the specifications required for 5G applications. The MSE measures how well a regression line fits a set of data points. It is a widely used metric for assessing the accuracy of a regression model's predictions. MSE calculates the average of the squared differences between predicted values and actual values, providing a measure of prediction error. Equation (6) presents the MSE formulation [39].

$$MSE = \frac{1}{n}\sum_{i=1}^{n}(\hat{y}_i - y_i)^2 \tag{6}$$

where $\hat{y}_i$ is the predicted value, y_i is the actual value, and n is the number of samples.

RMSE measures a regression model's accuracy by indicating the average magnitude of error between predicted and actual values. A lower RMSE signifies better performance. Unlike MSE, RMSE expresses errors in the original units, enhancing interpretability. Equation (7) shows its formulation [40].

$$RMSE = \sqrt{MSE} = \sqrt{\frac{1}{n}\sum_{i=1}^{n}(\hat{y}_i - y_i)^2} \tag{7}$$

R-squared (R^2), also known as the coefficient of determination, is a statistical metric that measures how well a regression model explains the variability of the target variable. It represents the proportion of the variance in the dependent variable that is predictable from the independent variables.

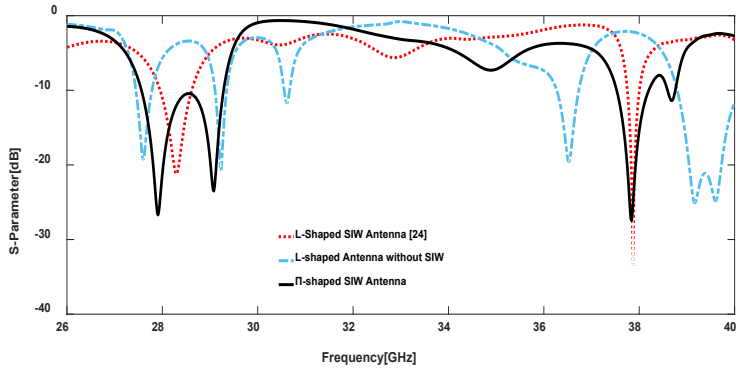

Figure 6. Reflection coefficient, S_{11}, results comparing with the L-shaped antenna without SIW, the L-shaped SIW antenna from [24], and the Π-shaped SIW antenna design.

Equation (8) depicts the formulation of R^2[40].

$$R^2 = 1 - SS_{res}/SS_{tot} \tag{8}$$

where SS_{res} is the residual sum of squared $\sum_{i=1}^{n}(y_i - \hat{y}_i)^2$, and SS_{tot} is the total sum of squared $\sum_{i=1}^{n}(y_i - \bar{y}_i)^2$.

4. RESULTS AND DISCUSSION

4.1 Analysis of Π-Shaped Slotted SIW Antenna Design

The Π-shaped slotted SIW antenna has been developed through a series of design enhancements, building upon the L-shaped antenna structures and incorporating a longitudinal slot to optimize performance for 5G applications. The validation of this design is based on comparisons with previous models, including the L-shaped patch antenna without the SIW and the L-shaped SIW antenna, as detailed in [24]. The return loss, quantified by the S_{11} parameter, is a critical measure of how much power is reflected from an antenna due to impedance mismatches or structural discontinuities. The main focus of this study is to demonstrate improvements in the reflection characteristics with the Π-shaped SIW antenna compared to its predecessors. As shown in Figure 6, simulations were conducted for three configurations: the L-shaped antenna without SIW, the L-shaped SIW antenna from [24], and the Π-shaped SIW antenna with the longitudinal slot. The dual-band resonant behavior observed at 28 GHz and 38 GHz for all three antenna designs is shown in Figure 6. Remarkably, the L-shaped SIW antenna outperforms the design without SIW, confirming that the incorporation of SIW enhances performance. This result validates the simulation methodology from [24], indicating that the reference L-shaped SIW antenna is a reliable baseline for performance comparisons.

However, the Π-shaped SIW antenna demonstrates significant improvements over the L-shaped SIW antenna from [24], achieving deeper return loss minima at both resonant frequencies (28 GHz and 38 GHz). This is a result of adding the longitudinal slot to the L-shaped structure, which optimizes current distribution and improves impedance matching. These changes contribute to the Π-shaped antenna's broader bandwidth and lower return loss, enhancing its performance relative to previous designs. Despite the improved performance of the Π-shaped design, further refinements in the antenna parameters, as discussed in Section 4.2, are required to fully optimize the configuration. However, the Π-shaped SIW antenna is already positioned as a highly promising candidate for 5G applications, offering better impedance matching, enhanced return loss, and broader bandwidth compared to earlier designs.

4.2 Results of Parametric Analysis

4.2.1 Effects of Varying Longitudinal and Transversal Slot Dimensions

A. Analysis of Simulated Results for Varying Length (L_1) and Width (W_1) of Longitudinal Slot

Figure 7(a) illustrates the effect of varying the length (L_1) and width (W_1) of Slot 1 on the antenna's performance while maintaining constant dimensions for the other two slots. The simulation results reveal that adjusting the length of Slot 1 from 7.8 mm to 8.6 mm allows the antenna to resonate at both 28 GHz and 38 GHz, with different return losses. When L_1 = 7.82 mm and W_1 = 0.66 mm, the return loss was -42.23 dB at 27.53 GHz and -32.85 dB at 37.78 GHz. In contrast, the worst performance was observed when L_1 = 7.84 mm and W_1 = 0.72 mm, with return losses of -20.92 dB and -29.75 dB at the respective frequencies. Optimal performance was achieved with L_1 = 7.9 mm and W_1 = 0.7 mm, where the reflection coefficients reached -60 dB at 27.83 GHz and -37.6 dB at 37.76 GHz, indicating the best impedance matching across both frequency bands. This analysis demonstrates that the configuration with L_1 = 7.9 mm and W_1 = 0.7 mm offers superior performance for both 28 GHz and 38 GHz. Thus, the optimal combination of L_1 = 7.9 mm and W_1 = 0.7 mm was selected, delivering improved bandwidth and significantly lower return loss compared to other configurations. However, the final antenna design will be determined following further analysis of multiple parameters, as discussed in Section 4.2.1(B).

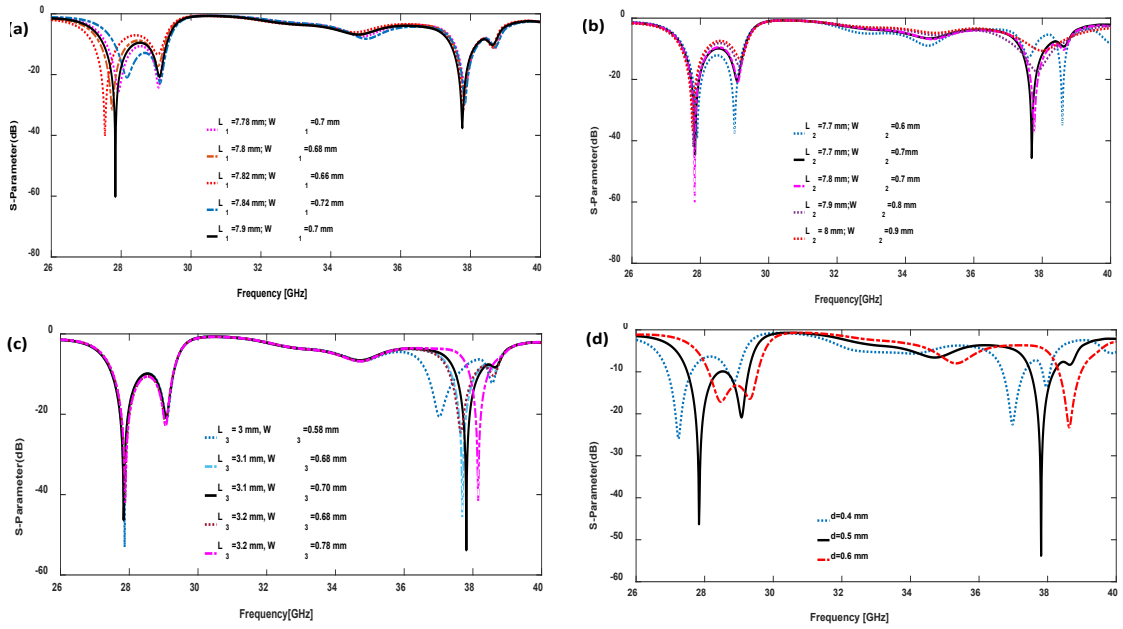

Figure 7. Parametric analysis results showing the impact of varying antenna parameters: (a) Length and width of the first longitudinal slot (L_1, W_1), (b) Length and width of the second longitudinal slot (L_2, W_2), (c) Length and width of the transverse slot (L_3, W_3), and (d) Diameter (d) of the vias on antenna performance.

B. Optimization of the Length (L_2) and Width (W_2) of Longitudinal Slot

Figure 7(b) provides a detailed comparison of the antenna's performance based on variations in the length (L_2) and width (W_2) of the second longitudinal slot. In these simulations, the slot length (L_2) was incrementally adjusted from 7.7 mm to 8 mm, while the width (W_2) was varied from 0.6 mm to 0.9 mm, with all other parameters, including the dimensions of the other slots and the overall antenna structure, kept constant. The results indicate that the antenna resonates at 27.89 GHz and 38.59 GHz, with reflection coefficients of -39.02 dB and -35.18 dB, respectively. A minimal reflection coefficient was observed when L_2 = 8 mm and W_2 = 0.9 mm, with return losses of -36.97 dB at 37.77 GHz and -10.64 dB at 38.02 GHz. The optimal performance, characterized by significantly improved impedance matching and reduced return losses, was achieved when the slot length (L_2) was set to 7.7 mm, and the width (W_2) to 0.7 mm, resulting in reflection coefficients of -44.2 dB at 27.84 GHz and -45.5 dB at 37.69 GHz. This configuration ensures efficient operation within the dual-band spectrum, minimizing energy losses and enhancing overall performance. As a result, the dimensions of L_2 = 7.7 mm and W_2= 0.7 mm were selected as the optimal parameters for the second longitudinal slot. These findings highlight the importance of fine-tuning design elements to achieve optimal electromagnetic performance, which will inform further antenna development, as detailed in Section 4.2.1(C).

C. Optimization of the Length (L_3) and Width (W_3) of Transversal Slot

The performance comparison of the antenna based on variations in the length (L_3) and width (W_3) of the transverse slot is shown in Figure 7(c). The simulation results demonstrate that the transverse slot's dimensions are crucial in tuning the antenna's resonances to the target frequencies of 28 GHz and 38 GHz. By adjusting the slot length (L_3) from 3.0 mm to 3.2 mm and varying the width (W_3) from 0.68 mm to 0.78 mm, the antenna achieves enhanced bandwidth, gain, and radiation efficiency. The return loss is minimized when the slot length is set to 3.2 mm and the width to 0.68 mm, with reflection coefficients of -42.2 dB at 27.87 GHz and -24.53 dB at 37.64 GHz. Importantly, setting the slot length to 3.1 mm and the width to 0.7 mm results in even greater performance, with return losses of -46.29 dB at 27.83 GHz and -53.82 dB at 37.81 GHz, indicating excellent performance at both frequencies. As a result, the optimal slot dimensions were selected as L_3 = 3.1 mm and W_3= 0.7 mm. While these findings showcase the potential for optimizing antenna performance, the final design will be determined following a thorough analysis of multiple parameters, as outlined in Section 4.2.2.

4.2.2 Effect of Via Diameter Variation

Figure 7(d) illustrates the effect of varying via diameters on antenna performance, with other parameters held constant. When the diameter d is set to 0.4 mm, resonances occur at 27.23 GHz and 36.98 GHz with reflection coefficients of -25.96 dB and -22.57 dB, respectively. However, a significant improvement is observed with a diameter of 0.5 mm, as the resonances align closely with the target frequencies of 28 GHz and 38 GHz. This configuration exhibits substantially improved reflection coefficients of -46.29 dB at 27.83 GHz and -53.82 dB at 37.81 GHz, demonstrating highly effective performance for the intended application. Based on these findings, a via diameter of 0.5 mm was selected for the refined design. However, finalized design specifications and detailed performance analysis will be discussed in Section 4.3.

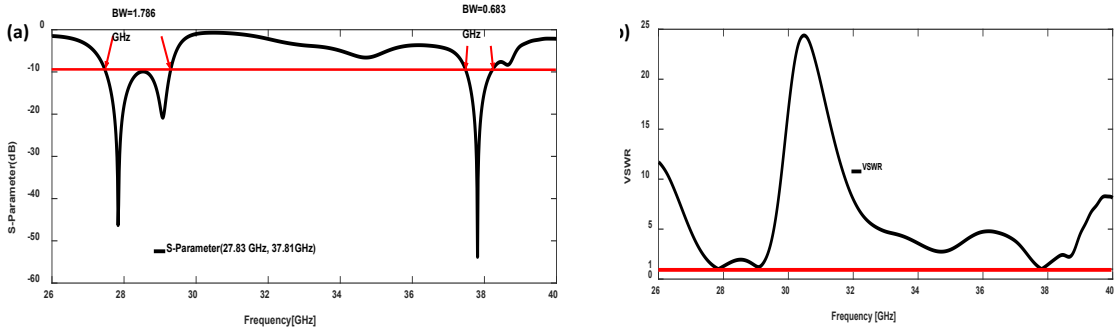

Figure 8. Simulation result of the optimized Π-shaped slotted antenna: (a) Return loss (S_{11}) and (b) VSWR.

4.3 Optimized Π-Shaped SIW Antenna Performance

4.3.1 Reflection Coefficient, VSWR Results, and Comparison with Reference Design

The optimized antenna's reflection coefficient is shown in Figure 8(a). CST software analysis reveals that the antenna exhibits dual resonances at 27.83 GHz and 37.81 GHz, with impressive return losses of -46.29 dB and -53.82 dB, respectively. Antenna bandwidth, which refers to the frequency range within which an antenna operates effectively, is typically defined using the -10 dB bandwidth criterion [28]. This standard indicates that the antenna effectively transmits or receives 90% of the power, with only 10% reflected to the source. The Fractional Bandwidth (FBW) for this antenna can be calculated using Equation (9), providing insight into its operational frequency range and overall performance characteristics.

$$FBW(\%) = \frac{(f_{max} - f_{min})}{f_c} \times 100 = \frac{BW}{f_c} \tag{9}$$

where f_{max} , f_c and f_{min} denotes the maximum, center, and minimum frequency of an antenna.

The Bandwidth Dimensions Ratio (BDR) is a key performance metric for antennas, providing insight into both miniaturization and bandwidth capabilities [28]. BDR measures the relationship between an antenna's physical size and its operational bandwidth. The BDR is determined by using the Equation (10)

$$BDR = \frac{BW(\%)}{\lambda_{length} \times \lambda_{width}} \tag{10}$$

Here, the Fractional Bandwidth, denoted as BW (%), is related to the antenna's electrical dimensions, where λ_{length} and λ_{width} represent the effective length and width of the proposed antenna, respectively. The electrical dimension of an antenna refers to its physical size relative to the operating wavelength λ_0 in free space [33]. It is a key parameter in antenna design, ensuring proper sizing for the intended frequency range while optimizing performance and scalability. The electrical dimension is given as

$$Electrical\ dimension = \frac{Physical\ dimension}{\lambda_o} \tag{11}$$

The optimized Π-shaped slotted antenna features two longitudinal slots that provide a wide bandwidth of 1.786 GHz, ranging from 27.491 GHz to 29.277 GHz, corresponding to a BW of 6.41% at the 27.83 GHz resonance frequency. Additionally, a transversal slot yields a bandwidth of 0.683 GHz, spanning from 37.498 GHz to 38.19 GHz, which equates to a fractional bandwidth of 1.81% at the 37.81 GHz resonance frequency. The antenna demonstrates excellent return losses of -46.29 dB and -53.82 dB at these respective resonance frequencies, indicating nearly perfect impedance matching between the antenna and the feeding element. The proposed antenna's wide bandwidths of 1.786 GHz and 0.683 GHz, coupled with reflection coefficients below -40 dB, make it highly effective for 5G mobile communication in the 28 GHz and 38 GHz bands. Figure 8(b) displays the Voltage Standing Wave Ratio (VSWR) of the optimized antenna, indicating how effectively signals are transmitted from the source to the antenna [29]. A low VSWR value reflects minimal signal reflection and optimal antenna performance. The VSWR values of 1.03 and 1.04 at their respective resonance frequencies demonstrate exceptional impedance matching, confirming the antenna's highly efficient design.

Figure 9 presents a comparative analysis of the performance between the proposed antenna and the reference antenna [24]. The optimized Π-shaped slotted antenna exhibits a significantly wider bandwidth of 1.786 GHz for the 28 GHz band, compared to 0.982 GHz for the reference, and a bandwidth of 0.683 GHz for the 38 GHz band, compared to 0.354 GHz for the reference antenna. Moreover, the optimized Π-shaped slotted antenna achieves significantly minimal return losses of -46.29 dB and -53.82 dB at the respective resonance frequencies, outperforming the reference antenna, which shows return losses of -17.346 dB and -34.397 dB**.** These enhancements underscore the proposed antenna's improved performance and greater efficiency compared to the reference design. The proposed antenna has electrical dimensions of 2.523λ₀ × 0.7λ₀ × 0.0237λ₀ at 27.85 GHz and 3.422λ₀ × 0.95λ₀ × 0.032λ₀ at 37.81 GHz, with a compact footprint of 27 × 7.5 × 0.254 mm.

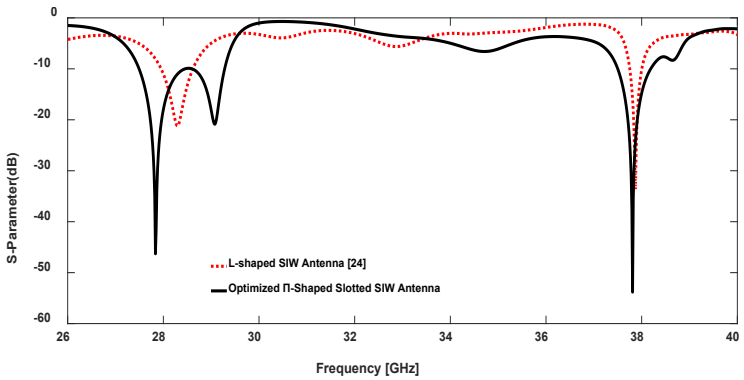

Figure 9. Comparing the reference L-shaped antenna [24] and the optimized Π-shaped slotted antenna.

4.3.2 Radiation Pattern Analysis of the Optimized Antenna

An antenna's radiation pattern, which is usually displayed in 2D or 3D formats, visually represents the distribution of electromagnetic fields or radiated power in different directions [30]. The E-plane ($\varphi = 0°$, *xz*-plane) and H-plane ($\varphi = 90°$, *yz*-plane) distributions of antenna radiation patterns indicate the polarization-dependent orientations of the Electric (*E*) and Magnetic (*H*) fields. For a patch antenna oriented along the *x*-axis, the magnetic field is orthogonal to the electric field and parallel to the patch width. The optimization of radiation patterns in antenna design primarily focuses on minimizing back lobes while maximizing forward gain through the main lobe, which is crucial for achieving optimal antenna performance. This approach enhances the Front-to-Back Ratio (F/B), improves directionality, and reduces unwanted side lobes, ultimately leading to better antenna efficiency and reduced interference. Several design techniques can be employed to mitigate this issue in slotted SIW antennas, where slots naturally tend to generate higher back radiation. These include strategic slot placement and orientation, implementation of reflecting surfaces, consideration of slot size and shape, incorporation of absorptive layers or backing structures, and thoughtful selection of substrate materials. The radiation pattern can be effectively controlled through the precise positioning of slots along the SIW structure and adding a metallic ground plane or reflective structure. Furthermore, utilizing substrates with low permittivity or high isolation materials can significantly reduce back radiation by preventing energy leakage through the substrate material. Figure 10(a) and (b) depict the antenna's uniform radiation patterns in the *E*- and *H*-planes at 27.83 GHz and 37.81 GHz, respectively. At 27.83 GHz, the *E*-plane exhibits a main lobe beamwidth of 68.8° with a -12.1 dB side lobe level, while the *H*-plane shows a 51.7° beamwidth and a -6.4 dB side lobe. At 37.81 GHz, both planes demonstrate a 61.3° beamwidth with a -14.4 dB side lobe level. The antenna's balanced radiation patterns and effective side lobe suppression across both frequency bands suit it for dual-band applications needing uniform coverage.

Figure 10(c) and (d) illustrate a 3D visualization of the optimized Π-shaped slotted antenna's gain distribution using a color gradient to show gain levels in dB across different angles. This provides an understandable and thorough view of the antenna's directional characteristics and overall radiation characteristics [26]. Red indicates higher gain, and blue indicates lower gain. The radiation pattern at 27.83 GHz is shown in Figure 11(c), where a larger peak gain of 7.9 dB is evident. This highlights the antenna's strong ability to concentrate energy in specific directions. The 3D gain plot at the second resonance frequency of 37.81 GHz is displayed in Figure 10(d). Compared to the pattern at 27.83 GHz, the antenna's radiation pattern at this frequency has a different peak gain of 8.05 dB and is more focused and directed despite the presence of many lobes that indicate strong emission in multiple directions.

The optimized Π-shaped slotted antenna's radiation efficiency over the frequency ranges between 27 and 40 GHz band is shown in Figure 11(a). The maximum radiation efficiency observed is 94.83% at 27.83 GHz, and it remains high at 92.61% at 37.81 GHz. However, the radiation efficiency drops to a minimum of 75.52% at 31 GHz. The optimized antenna's directivity and gain are shown for the same frequency range in Figure 11(b). Since gain results from multiplying radiation efficiency by directivity, an antenna has a larger gain when both parameters are high. According to the figure, the optimized antenna's gain and directivity at 27.83 GHz are 7.9 dB and 8.13 dB, respectively. Similarly, the directivity is 8.38 dB, and the gain is 8.05 dB at 37.81 GHz. Remarkably, the optimized antenna's maximum and lowest gain and directivity values are found at 31 and 39 GHz, respectively.

4.3.3 Surface Current Distribution of the Optimized Antenna

The distribution of electric current flowing on an antenna's conducting surfaces when stimulated by an electromagnetic signal or a linked source is referred to as surface current in antenna theory. Since the current distribution directly affects the patterns of the emitted electromagnetic field, it plays a crucial role in determining the radiation properties of the antenna. Antenna design optimization requires an understanding of surface current behavior since it affects critical performance parameters like radiation efficiency, directivity, and polarization [30]. The surface current patterns of the proposed dual-band Π-shaped SIW antenna reveal distinct characteristics at its resonant frequencies of 27.83 GHz and 37.81 GHz, visualized in Figure 12(a) and (b) using a color gradient from blue (minimal current) to red (maximal current). At the lower resonance of 27.83 GHz, current flows predominantly concentrated along the patch's longitudinal and transverse boundaries as well as the feed line, demonstrating how this frequency mode directs current through the central patch region and slot edges. The higher 37.81 GHz resonance exhibits more localized current distribution, with intense concentrations appearing in the patch center, slots, and feed lines, indicating enhanced resonant behavior and coupling efficiency.

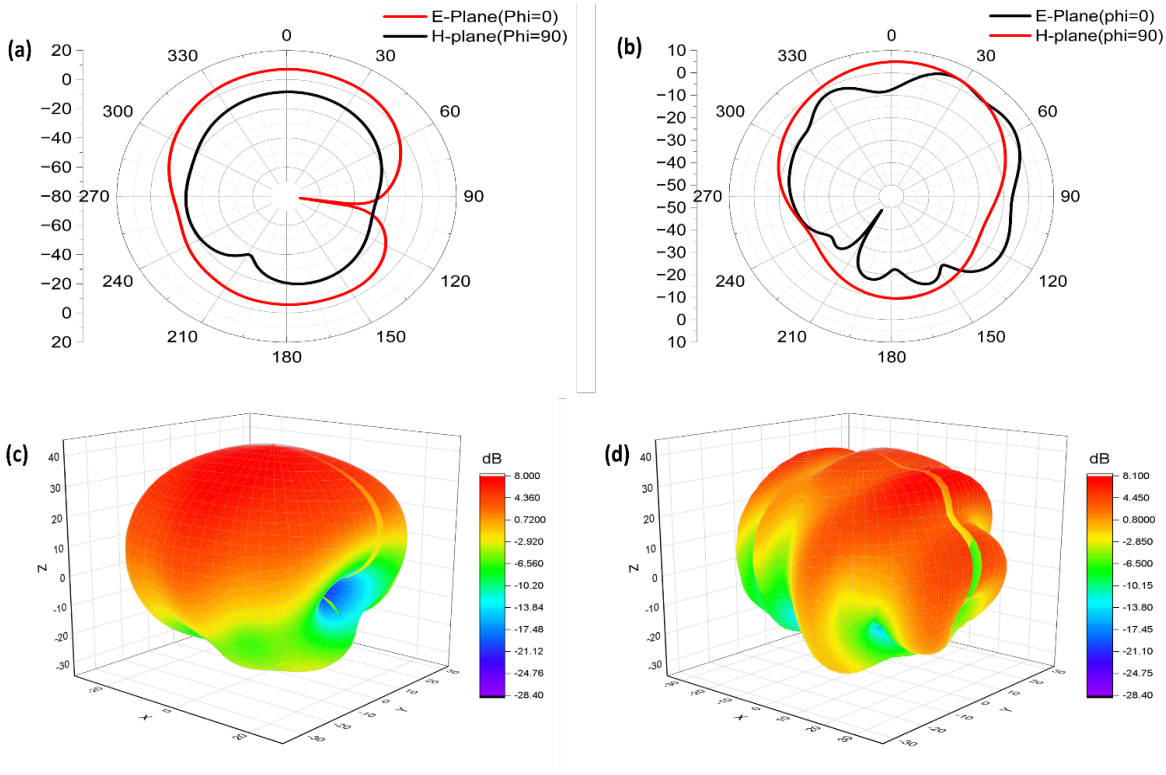

Figure 10. Radiation pattern for the optimized antenna of 2D view at (a) 27.83 GHz and (b) 37.81 GHz and 3D view at (c) 27.83 GHz (d) 37.81 GHz.

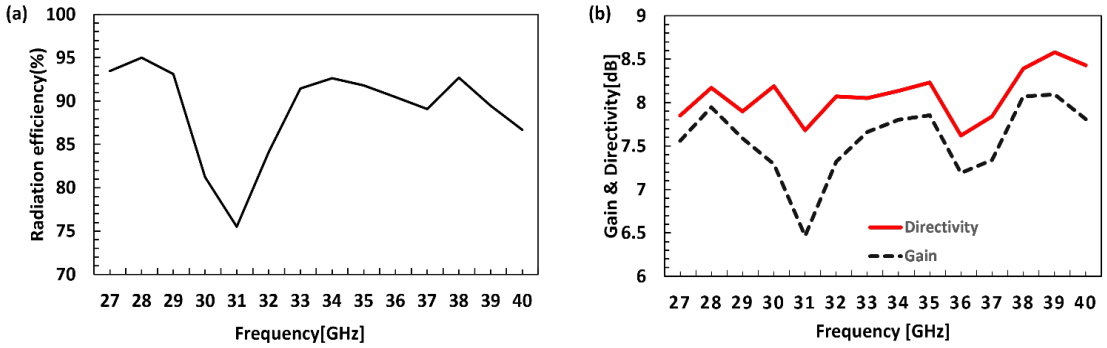

Figure 11. (a) Radiation efficiency and (b) gain and directivity of the optimized Π-shaped slotted antenna.

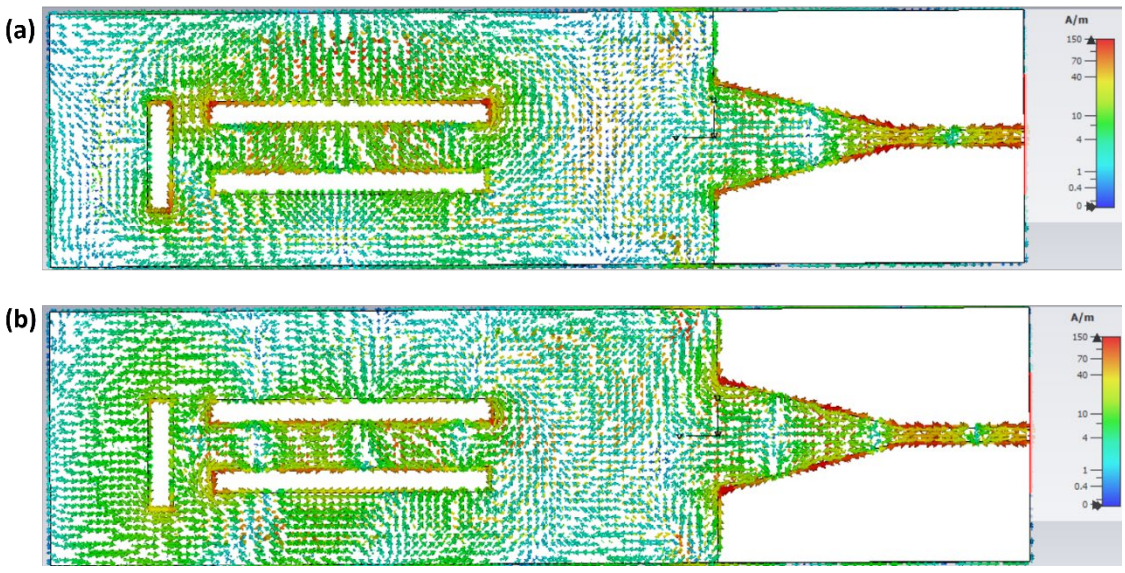

Figure 12. Optimized antenna's surface-current density at (a) 27.83 GHz and (b) 37.81 GHz.

4.4 ANN Predicted Results for Validation of CST Simulations

The ANN prediction results demonstrate a strong correlation with CST simulation data, providing robust validation of the proposed antenna design's performance across the targeted 28 GHz and 38 GHz 5G frequency bands. Statistical metrics such as Mean Absolute Error (MAE), MSE, RMSE, and R-squared are used to evaluate the model's effectiveness, as discussed in Section 3.4. The ANN model, trained using the Levenberg-Marquardt algorithm, showcases remarkable predictive capabilities, accurately estimating both resonance frequencies (f_1 and f_2) and gain values at the 28 GHz and 38 GHz bands. The model is trained with a dataset comprising 126 training samples, 16 testing samples, and 16 validation samples, achieving excellent precision across all significant parameters. The high coefficient of R-squared (R^2) values, further highlight the model's accuracy, which are 0.98 for f_1, 0.9428 for f_2, 0.97218 for the 28 GHz gain, and 0.93471 for the 38 GHz gain. The model's performance is further validated by its low error metrics. At the 28 GHz band, gain predictions yield an MSE of 0.001576 and an RMSE of 0.039698, while at the 38 GHz band, the MSE and RMSE are 0.022688 and 0.150625, respectively. Although the model exhibits slightly lower accuracy when predicting the second resonance frequency and gain at the 38 GHz band, these results reinforce the robustness and reliability of the ANN model in predicting critical performance metrics of the antenna design. Table 3 summarizes the performance metrics of the ANN model for resonance frequency and gain prediction.

The ANN model's performance is further illustrated in Figure 13, where the relationship between predicted outputs and target gain values for the proposed antenna is analyzed across various data subsets. These subsets include training, validation, and test sets, as well as the complete dataset. Each subplot presents data points, a regression line that shows the overall trend, and a diagonal line ($Y = T$) representing perfect correlation. For the 28 GHz gain, the ANN model achieves high R-values of 0.97374, 0.95785, 0.98555, and 0.97218 for the training, validation, test, and overall datasets, respectively. This indicates a strong alignment between predicted and actual values. Similarly, for the 38 GHz gain, the R-values are 0.92851, 0.93513, 0.98497, and 0.93471 across the corresponding data partitions. The consistently high correlation coefficients demonstrate the model's exceptional ability to predict the antenna's gain values with high reliability. Despite slight variations across the subsets, the model provides accurate predictions, proving invaluable for evaluating antenna performance in the 28/38 GHz 5G bands.

Table 3. Performance metrics of ANN models for resonance frequency and gain predictions.

Target	Training algorithm	Sample	Testing	Validation	MSE	RMSE	R^2
First resonance frequency (f_1)	Levenberg-Marquardt	126	16	16	0.0092	0.09591	0.98
Second resonance frequency (f_2)	Levenberg-Marquardt	126	16	16	0.0096	0.0979	0.9428
Gain for 28 GHz	Levenberg-Marquardt	126	16	16	0.001576	0.039698	0.97218
Gain for 38 GHz	Levenberg-Marquardt	126	16	16	0.022688	0.150625	0.93471

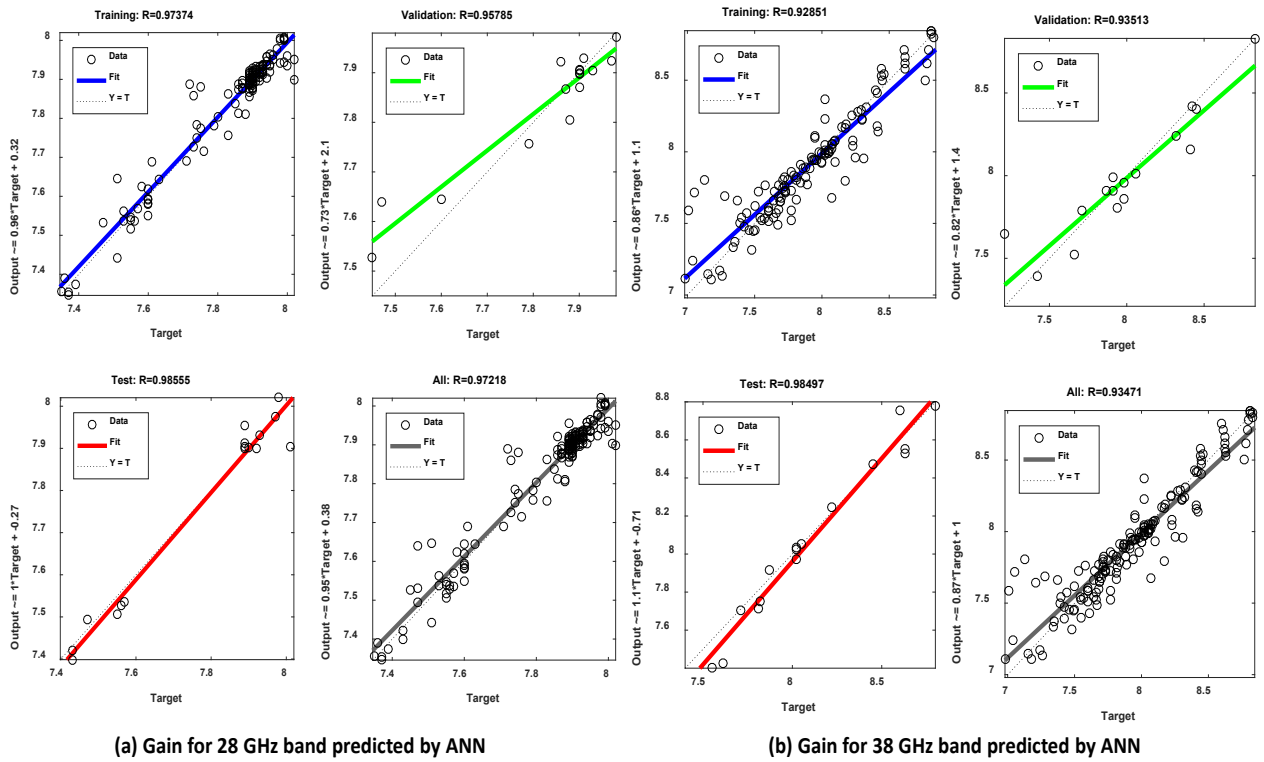

Figure 13. ANN model performance for gain at (a) 28 GHz band and (b) 38 GHz band.

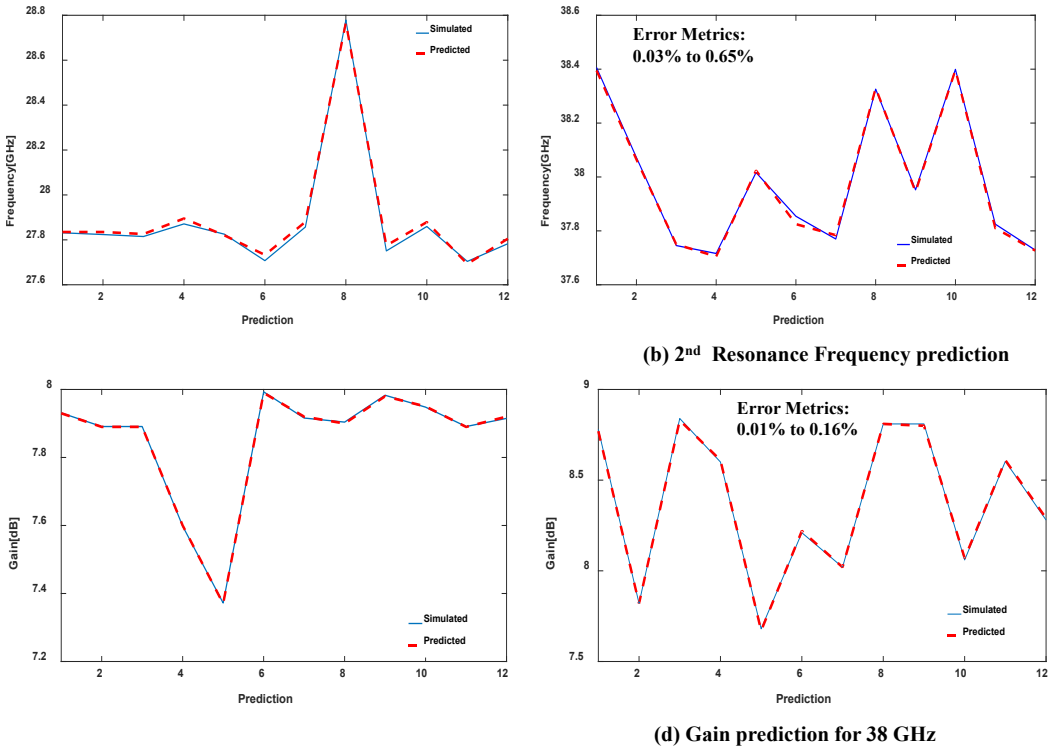

Figure 14. Validation of frequencies and gains for the 28 GHz and 38 GHz bands.

The validation of the frequencies and gains for the 28 GHz and 38 GHz bands is presented in Figure 14, where simulated results (blue curves) are compared with predicted outcomes (red curves). The close alignment of the curves underscores the model's ability to accurately capture frequency response characteristics, including peaks, valleys, and overall trends. Resonance frequency predictions show remarkable accuracy, with error margins as low as 0.00% to 0.43% for the 28 GHz band and 0.03% to 0.65% for the 38 GHz band. Gain predictions also exhibit exceptional precision, with minimal error variations of 0.01% to 0.05% at 28 GHz and 0.01% to 0.16% at 38 GHz, confirming the model's reliability in predicting significant antenna parameters.

5. COMPARISON WITH PRIOR RESEARCH ON 5G ANTENNAS

A comparative analysis of existing 5G antenna technologies highlights the proposed design's significant advantages, showcasing superior performance metrics, enhanced radiation efficiency, and exceptional suitability for 28 GHz and 38 GHz 5G applications. Table 4 provides a comprehensive comparison with similar antennas from recent literature, clearly establishing the proposed design's exceptional suitability for 28 GHz and 38 GHz 5G applications through detailed analysis of critical performance parameters including impedance matching, bandwidth, and radiation characteristics.

In case of return loss characteristics, a more negative return loss indicates superior impedance matching, which minimizes signal reflection and enhances the overall efficiency of the antenna. The proposed antenna design demonstrates the highest return loss among all referenced works, achieving -46.29 dB at 28 GHz and -53.82 dB at 38 GHz. These values significantly surpassed previous studies, where the best recorded return losses were -42 dB at 28 GHz [34] and -38.8 dB at 38 GHz [37]. This proposed antenna's improved impedance matching ensures better signal transmission and reception, making the proposed design highly suitable for 28 GHz and 38 GHz 5G applications.

In terms of bandwidth, the proposed design offers 1.786 GHz at 28 GHz and 0.683 GHz at 38 GHz. While it surpasses several previous designs including [31] (1.23 GHz at 28 GHz, 1.06 GHz at 38 GHz) and [32] (0.9 GHz at 28 GHz), it falls behind [38] (3.65 GHz at 28 GHz, 2.19 GHz at 38 GHz) and [36] (1.43 GHz at 28 GHz, 3.54 GHz at 38 GHz). Although [36] provides wider bandwidth, its gain performance (2.7 dB at 28 GHz, 6 dB at 38 GHz) falls significantly short of the proposed design (7.9 dB at 28 GHz, 8.05 dB at 38 GHz). While [38] demonstrates both wider bandwidth and higher gain, its design is notably more complex and challenging to implement compared to the proposed antenna structure.

In comparison to gain, the proposed antenna demonstrates strong performance, achieving 7.9 dB at 28 GHz and 8.05 dB at 38 GHz, making it one of the top-performing designs in the comparison. At 28 GHz, it outperforms several existing designs, including [31], [33], [35], [36], [37], and [24], while closely competing with [32] (8.4 dB) and falling slightly behind [38] (10.06 dB). Similarly, at 38 GHz, its gain surpasses multiple references, including [31], [32], [34], [36], and [37], while remaining competitive with [24] and [35]. Despite [38] exhibiting the highest gain, its complex design poses implementation challenges compared to the proposed structure. When evaluated holistically across all performance metrics, including return loss, bandwidth, and radiation efficiency, the proposed antenna offers a well-balanced and optimized solution, making it highly suitable for 5G applications.

Furthermore, while prior designs showcase promising features, the proposed Π-shaped slotted SIW antenna, which evolved from a modified L-shaped structure, offers a compelling solution for 5G mobile networks operating at 28 GHz and 38 GHz frequency bands. The incorporation of SIW technology successfully integrates waveguide structures into a microstrip antenna, delivering a compact and low-profile solution. The antenna's utilization of the dominant TE_{10} mode ensures excellent frequency selectivity and reduced interference from higher-order modes, while its robust SIW structure enhances mechanical stability under environmental stress. This work maintains a permittivity of 2.2, consistent with several prior studies, and achieves the highest measured radiation efficiency (MRE) at 94.83%, surpassing all other designs. These results highlight the design's excellent impedance matching, high gain, and superior efficiency, making it a strong candidate for high-frequency applications.

Table 4. Comparative analysis of performance with previous research.

Ref.	No. of Bands	Return loss (dB)		Bandwidth (GHz)		Gain (dB)		Permittivity (ε_r)	MRE (%)
		28 GHz	38 GHz	28 GHz	38 GHz	28 GHz	38 GHz		
[31]	2	-34.5	-27.3	1.23	1.06	6.60	5.86	3.0	90.3
[32]	2	-25.0	-26.0	0.90	2.00	8.40	6.10	2.2	N/A
[33]	2	-38.3	-30.8	1.34	2.26	7.20	7.65	2.2	94.0
[34]	2	-42.0	-19.0	0.50	0.70	8.21	5.74	2.2	94.0
[35]	2	N/A	N/A	N/A	N/A	4.15	7.73	3.0	85.44
[36]	2	-20.0	-15.0	1.43	3.54	2.70	6.00	4.67	N/A
[37]	2	-38.8	-37.2	1.53	2.21	6.95	5.20	2.2	N/A
[38]	2	-25.0	-12.0	3.65	2.19	10.06	10.20	2.2	75.75
[24]	2	-17.3	-34.3	0.982	0.354	7.05	8.32	2.2	90.0
This work	2	-46.29	-53.82	1.786	0.683	7.90	8.05	2.2	94.83

N/A: Not available; MRE: Maximum radiation efficiency.

6. CONCLUSION

This work successfully presents a Π-shaped slotted SIW antenna design that achieves dual-band operation for 28 GHz and 38 GHz through the innovative integration of longitudinal and transversal slots guided by vias. The antenna incorporates an advanced SIW via structure with a microstrip line feed, optimizing both gain and bandwidth. By strategically positioning longitudinal and transversal slots with guiding vias, it effectively manages electromagnetic waves, achieving bandwidths of 6.41% at 28 GHz and 1.81% at 38 GHz, along with realized gains of 7.9 dB and 8.05 dB for reliable signal transmission. Its single-layer construction facilitates seamless integration, while low return losses, a VSWR range between 1 and 5, and high radiation efficiency further enhance its practical applicability. The CST simulation results were successfully validated using an ANN model, confirming excellent performance with an MSE of 0.0092 and R^2 of 0.98 for frequency prediction, as well as an MSE of 0.001576 and R^2 of 0.97218 for 28 GHz band gain prediction. The SIW antenna demonstrates a compact design, excellent impedance matching, and strong gain performance, making it highly suitable for 5G mm-wave communication systems. Its stable dual-band operation at 28 GHz and 38 GHz offers a promising solution for applications such as wireless backhaul, small cell base stations, and high-speed point-to-point communication links. While the antenna delivers strong gain and efficiency, further enhancements are needed to meet the growing demands of high-speed wireless networks. Future research will focus on improving both gain and efficiency, along with integrating advanced beamforming networks for precise directional control, enhanced spatial multiplexing, and effective interference mitigation. These advancements will drive the evolution of next generation 6G wireless technologies, ensuring more efficient and high-performance communication systems

ACKNOWLEDGMENT AND FUNDING

The authors thank the Universiti Malaysia Pahang Al-Sultan Abdullah for laboratory facilities and financial support under Internal Research Grant RDU220382.

DECLARATION OF CONFLICTING INTERESTS

The authors declare no potential conflicts of interest with respect to the research and publication of this article.

REFERENCES

[1] B. A. F. Esmail and S. Koziel, Design and optimization of metamaterial-based dual-band 28/38 GHz 5G MIMO antenna with modified ground for isolation and bandwidth improvement, *IEEE Antennas and Wireless Propagation Letters*, 5, 2022, 1069-1073.

[2] E. H. Orallo, M. M. Arcila, J.C. Cano, C. T. Calafate, J. A Conejero and P. Manzoni, An analytical model based on population processes to characterize data dissemination in 5G opportunistic networks, *IEEE Access,* 6, 2017, 1603-1615.

[3] J. H. Lee, J. S. Choi and S. C. Kim, Cell coverage analysis of 28 GHz millimeter wave in urban microcell environment using 3-D ray tracing, *IEEE Transactions on Antennas and Propagation,* 3, 2018, 1479-1487.

[4] B. Yang, Z. Yu, Y. Dong, J. Zhou and W. Hong, Compact tapered slot antenna array for 5G millimeter-wave massive MIMO systems. *IEEE Transactions on Antennas and Propagation*, 12, 2017, 6721-6727.

[5] T. S. Rappaport, S. Sun, R. Mayzus, H. Zhao, Y. Azar, K. Wang, G. N. Wong, J. K. Schulz, M. Samimi and F. Gutierrez, Millimeter wave mobile communications for 5G cellular: it will work!, *IEEE Access*, 1, 2013, 335-49.

[6] J. F. Zhang, Y. J. Cheng, Y. R. Ding and C. X. Bai, A dual-band shared-aperture antenna with large frequency ratio, high aperture reuse efficiency, and high channel isolation, *IEEE Transactions on Antennas and Propagation*, 2, 2018, 853-60.

[7] C. Han, Y. Bi, S. Duan and G. Lu, Rain rate retrieval test from 25-GHz, 28-GHz, and 38-GHz millimeter-wave link measurement in Beijing, *IEEE Journal of Selected Topics in Applied Earth Observations and Remote Sensing*, 8, 2019, 2835-47.

[8] M. M. Alam, A. A. F. Faudzi, S. M. Shaharum, Y. A. Wahab, M. H. A. A. Malek, M. S. A. Karim and N. A. T. Yusof, Design and analysis of triple-band SIW antenna for K-Band and Ka-Band applications, *International Exchange and Innovation Conference on Engineering & Sciences*, Japan, 2024.

[9] W. M. A. Wahab and S. S. Naeini, Wide-bandwidth 60-GHz aperture-coupled microstrip patch antennas (MPAs) fed by substrate integrated waveguide (SIW), *IEEE Antennas and Wireless Propagation Letters,*10, 2011, 1003-1005.

[10] D. Deslandes and K. Wu, Accurate modeling, wave mechanisms, and design considerations of a substrate integrated waveguide, *IEEE Transactions on Microwave Theory and Techniques*, 6, 2006, 2516-2526.

[11] I. Serhsouh, M. Himdi, H. Lebbar and H. Vettikalladi, Reconfigurable SIW antenna for fixed frequency beam scanning and 5G applications, *IEEE Access,* 8, 2020, 60084-60089.

[12] Z. Pi and F. Khan, An introduction to millimeter-wave mobile broadband systems, *IEEE Communications Magazine*, 6, 2011, 101-107.

[13] T. Li and Z. N. Chen, Shared-surface dual-band antenna for 5G applications, *IEEE Transactions on Antennas and Propagation*, 2, 2019, 1128-1133.

[14] K. A. Amoodi, R. Mirzavand, M. M. Honari, J. Melzer, D. G. Elliott and P. Mousavi, A compact substrate integrated waveguide notched-septum polarizer for 5G mobile devices, *IEEE Antennas and Wireless Propagation Letters*, 12, 2020 2517-2521.

[15] C. Yu and W. Hong, 37–38 GHz substrate integrated filtenna for wireless communication application, *Microwave and Optical Technology Letters*, 2, 2012, 346-351.

[16] T. Hong, Z. Zhao, W. Jiang, S. Xia, Y. Liu and S. Gong, Dual-band SIW cavity-backed slot array using TM 020 and TM 120 modes for 5G applications, *IEEE Transactions on Antennas and Propagation*, 5, 2019, 3490-3495.

[17] F. P. Lai, L. W. Chang and Y. S. Chen, Miniature dual-band substrate integrated waveguide slotted antenna array for millimeter-wave 5G applications, *International Journal of Antennas and Propagation*, 1, 2020, 6478272.

[18] L. Kumar, V. Nath and B. V. R. Reddy, A wideband substrate integrated waveguide (SIW) antenna using shorted vias for 5G communications, *AEU-International Journal of Electronics and Communications*, 171, 2023, 154879.

[19] L. Sabri, N. Amiri and K. Forooraghi, Dual-band and dual-polarized SIW-fed microstrip patch antenna, *IEEE Antennas and Wireless Propagation Letters*, 13, 2014, 1605-1608.

[20] G. Q. Luo, Z. F. Hu, L. X. Dong and L. L. Sun, Planar slot antenna backed by substrate integrated waveguide cavity, *IEEE Antennas and Wireless Propagation Letters,* 7, 2008, 236-239.

[21] F. Xu and K. Wu., Guided-wave and leakage characteristics of substrate integrated waveguide, *IEEE Transactions on Microwave Theory and Techniques*, 1, 2005, 66-73.

[22] N. S. Khair, N. A. T. Yusof, Y. A. Wahab, B. S. Bari, N. I. Ayob and M. Zolkapli, Substrate-integrated waveguide (SIW) microwave sensor theory and model in characterising dielectric material: A review, *Sensors International*, 2023 100244.

[23] T. Zhang, W. Hong, Y. Zhang, and K. Wu., Design and analysis of SIW cavity backed dual-band antennas with a dual-mode triangular-ring slot, *IEEE Transactions on Antennas and Propagation*, 10, 2014, 5007-5016.

[24] J. Singh, F. L. Lohar and B. S. Sohi, Design of dual band millimeter wave antenna using SIW material for 5G cellular network applications, *Materials Today: Proceedings*, 45, 202, 5405-5409.

[25] X. Li, J. Xiao, Z. Qi and H. Zhu., Broadband and high-gain SIW-fed antenna array for 5G applications, *IEEE Access*, 6, 2018, 56282-56289.

[26] F. Gil, A. R. Claro, J. M. Ferreira, C. Pardelinha and L. M. Correia, A 3D interpolation method for base-station-antenna radiation patterns, *IEEE Antennas and Propagation Magazine*, 2, 2001, 132-137.

[27] S. Mukherjee, A. Biswas and K. V. Srivastava, Substrate integrated waveguide cavity-backed dumbbell-shaped slot antenna for dual-frequency applications, *IEEE Antennas and Wireless Propagation Letters*, 14, 2014, 1314-1317.

[28] G. Q. Luo, Z. F. Hu, W. J. Li, X. H. Zhang, L. L. Sun and J. F. Zheng, Bandwidth-enhanced low-profile cavity-backed slot antenna by using hybrid SIW cavity modes, *IEEE Transactions on Antennas and Propagation*, 4, 2012, 1698-1704.

[29] H. Nakano, M. Fukasawa, and J. Yamauchi, Discrete multiloop, modified multiloop and plate-loop antennas-multifrequency and wideband VSWR characteristics, *IEEE Transactions on Antennas and Propagation*, 3, 2002, 371-378.

[30] M. Ortiz, M. N. Uddin, M. R. Guerra and E. A. Alwan, Enhancing gain through optimal antenna element distribution in a thinned array configuration, *IEEE Open Journal of Antennas and Propagation*, 4, 2023, 1176-1186.

[31] A. E. Farahat and K. F. A. Hussein, Dual-band (28/38 GHz) wideband MIMO antenna for 5G mobile applications, *IEEE Access,* 10, 2022, 32213-32223.

[32] P. Liu, X. W. Zhu, Y. Zhang, X. Wang, C. Yang and Z. H. Jiang, Patch antenna loaded with paired shorting pins and H-shaped slot for 28/38 GHz dual-band MIMO applications, *IEEE Access*, 8, 2020, 23705-23712.

[33] M. M. Diallo, D. B. O. Konditi and O. V. Bossou, A miniaturized dual-band planar antenna with a square ring defected ground structure for 5G millimetre-wave applications, *Indonesian Journal of Electrical Engineering and Computer Science*, 1, 2023, 197-205.

[34] S. K. Gupta and A. Bage, A compact, dual-band antenna with defected ground structure for 5G applications, *Journal of Circuits, Systems and Computers*, 16, 2021, 2150298.
[35] R. N. Tiwari, D. Sharma, P. Singh and P. Kumar, A flexible dual-band 4× 4 MIMO antenna for 5G mm-wave 28/38 GHz wearable applications, *Scientific Reports*, 1, 2024, 14324.
[36] S. Muhammad, I. Ya'u, A. S. Abubakar and A. S. Yaro, Design of single feed dual-band millimeter wave antenna for future 5G wireless applications, *Science World Journal*, 1, 2019, 84-87.
[37] S. A. Refaat, H. A. Mohamed, A. M. Abdelhady and A. S. Mohra, A 28/38 GHz tuned reconfigurable antenna for 5G mobile communications, *Indonesian Journal of Electrical Engineering and Computer Science*, 1, 2023, 248.
[38] T. Deckmyn, M. Cauwe, D. V. Ginste, H. Rogier and S. Agneessens, Dual-band (28, 38) GHz coupled quarter-mode substrate-integrated waveguide antenna array for next-generation wireless systems, *IEEE Transactions on Antennas and Propagation*, 4, 2019, 2405-2412.
[39] M. A. Haque, M. A. Rahman, S. S. A. Bawri, K. Aljaloud, N. S. S. Singh, D. Saha, E. E. Hussin, W. M. Abdulkawi and M. A. Zakariya, Machine learning-based approach for bandwidth and frequency prediction for N77 band 5G antenna, *Physica Scripta*, 99(2), 2024, 026005.
[40] M. S. Rana, S. M. R. Islam and S. Sarker, Machine learning based on patch antenna design and optimization for 5G applications at 28 GHz, *Results in Engineering*, 24, 2024, 103366.